

Article

Effect of N Content on the Microstructure and Impact Properties of Normalized Vanadium Micro-Alloyed P460NL1 Steel

Xinliang Li ^{1,2}, Huibing Fan ², Qiuming Wang ¹ and Qingfeng Wang ^{1,3,4,*}

¹ State Key Laboratory of Metastable Materials Science and Technology, School of Materials Science Technology and Engineering, Yanshan University, Qinhuangdao 066004, China; 18332576552@163.com (Q.W.)

² Nanjing Iron & Steel Co., Ltd., Nanjing 211500, China

³ National Engineering Research Center for Equipment and Technology of Cold Strip Rolling, School of Mechanical Engineering, Yanshan University, Qinhuangdao 066004, China

⁴ Hebei Key Lab for Optimizing Metal Product Technology and Performance, School of Materials Science Technology and Engineering, Yanshan University, Qinhuangdao 066004, China

* Correspondence: wqf67@ysu.edu.cn

Abstract: In this work, the effect of nitrogen doping on vanadium micro-alloyed P460NL1 steel is studied in terms of microstructures and impact toughness. As the nitrogen content increased from 0.0036% to 0.0165%, the number of V (C,N) particles increased. The fine precipitates of V (C,N) effectively pin the prior austenite grain boundary, resulting in the refinement of the austenite grain. The intragranular and intergranular V-containing coarse particles enhanced the nucleation of intragranular ferrite and the grain boundaries of polygonal ferrite during air cooling. Accordingly, the proportion of heterogeneously nucleated ferrite increased, and the grain size of ferrite decreased. Notably, the size of the pearlite microstructure decreased, and the bainite microstructure appeared with a high doping of N. With the increase in N content, the impact toughness of vanadium micro-alloyed P460NL1 steel was enhanced. This can be attributed to the refinement of ferrite and the reduction in pearlite, which, in turn, was ascribed to the increase in nitrogen.

Keywords: N content; P460NL1; microstructure; impact toughness



Citation: Li, X.; Fan, H.; Wang, Q.; Wang, Q. Effect of N Content on the Microstructure and Impact Properties of Normalized Vanadium Micro-Alloyed P460NL1 Steel. *Metals* **2023**, *13*, 1896. <https://doi.org/10.3390/met13111896>

Academic Editors: Rebecca L. Higginson and Hardy Mohrbacher

Received: 14 September 2023
Revised: 19 October 2023
Accepted: 31 October 2023
Published: 16 November 2023



Copyright: © 2023 by the authors. Licensee MDPI, Basel, Switzerland. This article is an open access article distributed under the terms and conditions of the Creative Commons Attribution (CC BY) license (<https://creativecommons.org/licenses/by/4.0/>).

1. Introduction

Advances in equipment and the rapid development of the application of the thermo-mechanical control process (TMCP) in the metallurgical industry have promoted the use of hot-rolled micro-alloyed steel due to its good mechanical performance [1]. Notably, normalized steel sheets with stabilized microstructures are preferred in specific fields, including high-pressure vessels and tank trucks [2]. High-strength normalized steel sheets can enhance building quality and reduce the dead weight of steel structures. There is a substantial demand for normalized steel with good mechanical performance. However, normalizing eliminates the fine structure obtained by controlled rolling and controlled cooling, and the strengthening method is limited for normalized steel. Currently, the strength improvement of normalized steel sheets relies on alloying [3,4].

In this context, V-N micro-alloying has proven to be an effective method for material reinforcement, especially for thick sheets [5–9]. Due to the strong precipitation-strengthening effect of V (C,N) particles in the steel, V/V-N micro-alloying has been widely employed in hot-rolled products, including steel bars, thin plate continuous casting and rolling strips, structural steel, seamless steel pipes, etc. [10,11].

Normalizing modifies the quantity, size, and distribution of V (C,N) precipitates, thereby influencing the mechanical behavior of steel [12–14]. In V micro-alloyed steels, the majority of VC particles dissolve in austenite during normalizing. In V-N micro-alloyed steel, the thermal stability of V (C,N) particles can be significantly improved by incorporating N content, and some V (C,N) precipitates remain in the steel during

normalizing [3,11]. The undissolved V (C,N) precipitates fix the austenite boundary during the holding stage of the normalizing process, resulting in the refinement of the austenite grain. Additionally, the undissolved V (C,N) provides nucleation sites for ferrite during the subsequent cooling stage [15–18]. As a result, the microstructure is further refined, and good mechanical performance is achieved. However, the N content in solid solution increases with the increasing N content in V-N micro-alloyed steel, which may deteriorate the impact toughness of the steel [19]. Unfortunately, there have been few systematic research reports on the influence of N content on the microstructure and impact properties of V-N micro-alloyed normalized steel. The effect of N content on the microstructure and impact toughness of V-N micro-alloyed normalized steel remains unclear.

In this study, the effect of an increase in N content from 0.0036% to 0.0165% on the microstructure and impact properties of normalized V micro-alloyed P460NL1 steel was systematically studied. This guides the development of normalized vanadium–nitrogen micro-alloyed high-strength P460NL1 steel.

2. Materials and Methods

2.1. Materials

To study the effects of N content on the microstructure and impact properties of normalized vanadium micro-alloyed P460NL1 steel, 3 furnaces with different N-content steels were smelted using a 150 kg vacuum furnace in the laboratory. The N content of the steel in the three furnaces was 0.0036%, 0.0103%, and 0.0165%, respectively. The specific chemical composition of the experiment steels is shown in Table 1. The liquid steel was cast into cuboid ingots with dimensions of 220 mm (thickness) × 260 mm (width) × L mm (length). Subsequently, the ingots were heated to 1200 °C for 2 h using a resistance furnace and then rolled into 24-millimeter-thick steel sheets with a 350 mm hot roller under a controlled rolling process. The three steels were naturally cooled to room temperature and then used as test materials for this study.

Table 1. Components of experimental steels.

Steel	C	Si	Mn	P	S	Ni	V	N	Alt
36N	0.182	0.26	1.63	0.010	0.002	0.51	0.159	0.0036	0.002
103N	0.180	0.27	1.65	0.010	0.002	0.50	0.155	0.0103	0.004
165N	0.183	0.26	1.70	0.009	0.002	0.51	0.162	0.0165	0.008

2.2. Method

2.2.1. Heat Treatment

Samples measuring 24 mm × 300 mm × 350 mm were cut from each rolled steel sheet. These were heated to 900 °C in a chamber resistance furnace (YIANJIE ELECTRIC FURNACE INDUSTRY Co., Ltd., Luo Yang, China) and held at this temperature for 30 min. Then, the samples were removed from the chamber resistance furnace and air-cooled to room temperature. The specific process of the normalizing treatment is shown in Figure 1a. To study the evolution process of precipitation during the normalizing process, as well as phase transitions, the following thermal process was simulated using the Gleeble 3800 thermal simulator (Dynamic Systems Inc., New York, NY, USA). One pair of samples was heated to 900 °C at a rate of 5 °C/s and held at 900 °C for 30 min. Then, the sample was rapidly water-quenched to 20 °C. The other pair of samples was heated to 900 °C at a rate of 5 °C/s and also held at 900 °C for 30 min. and then the sample cooled to 880 °C, as illustrated by the dotted lines in Figure 1b, subsequently, the sample was water-quenched to 20 °C.

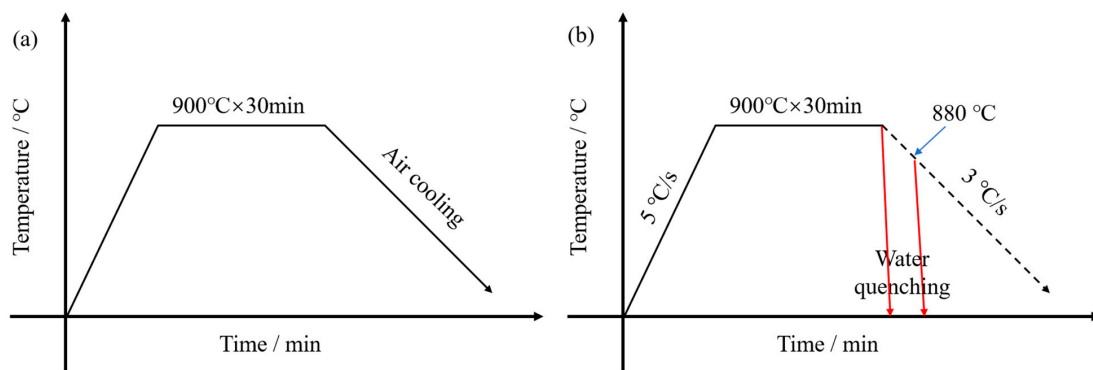


Figure 1. Schematic diagram of the normalizing process and simulated thermal cycle processes: normalizing process (a); simulated thermal cycle processes on Gleeble 3800 (b).

2.2.2. Mechanical Properties Test

Round bar tensile specimens with a diameter of 10 mm and three impact specimens, each with a standard size of 10 mm × 10 mm × 55 mm, were processed along the transverse direction from three normalized steel plates with different N contents. The impact energy of the samples with varying N contents at $-40\text{ }^{\circ}\text{C}$ was tested using a JBN-300B pendulum impact testing machine (DENGCE YIQI Co., Ltd., Jinan, China). Three groups of impact specimens were tested for each type of steel, and the average value of the impact energy from the three tests was calculated to minimize testing errors. Scanning electron microscopy was used to observe the fracture morphology of the steel samples with different N contents. Tensile tests were carried out using the GX-B03A testing machine (CITEMA Co., Ltd., Shanghai, China) with an extension rate of 3 mm/min at room temperature to determine the tensile properties of the test samples.

2.2.3. Microstructure

Metallographic sections were taken from the normalized samples with different N contents. These sections underwent mechanical polishing, were etched with a 4% nitric acid alcohol solution for 5 s, and were then observed under an Olympus BX51M optical microscope (Olympus, Aizu, Japan). Following this observation, the metallographic sections were repolished, and the samples were electropolished in an electrolyte. The electropolished samples were scanned using electron backscatter diffraction (EBSD, Hitachi Limited, Tokyo, Japan), and the effective grain size of the samples with different N contents was calculated using OIM analysis 9 software (Hitachi Limited, Tokyo, Japan). The effective grain size is defined according to the misorientation angle of adjacent grains. Microstructure observations of water-quenched samples were conducted using the S-3400 scanning electron microscope (SEM, Hitachi Limited, Tokyo, Japan). The fine precipitates and microstructure characteristics were further investigated via JEM-2010 high-resolution transmission electron microscopy (TEM, Japan Electronics optics Corporation, Tokyo Prefecture, Japan) by using extraction replicas of C films and thin foil samples. In addition, energy-dispersive X-ray spectroscopy (EDS, Hitachi Limited, Tokyo, Japan) was used to perform a compositional analysis of the precipitates. Additionally, SEM and EBSD were used to observe secondary cracks in impacted samples to clarify the correlation between microstructure and impact failure.

3. Results and Discussion

3.1. Effect of N Content on the Microstructures of Steel Samples

Figure 2 shows the microstructure of vanadium micro-alloyed P460NL1 steel sheets normalized at $900\text{ }^{\circ}\text{C}$. As observed, the 36N sample consists of ferrite and pearlite; the 103N and 165N samples consist of ferritic pearlite and bainitic ferrite, with bainitic ferrite distributed in bands. As N doping increases, the amount of pearlite decreases while bainitic ferrite increases. In addition, the grains are refined and distributed more uniformly. Image-

pro was used to measure the proportion of each type of microstructure. With the N content increasing from 36 ppm to 103 ppm, the pearlite phase decreases from 8.3% to 3.2%, and bainitic ferrite increases to 15.5%. As the N content further increases from 103 ppm to 165 ppm, the pearlite phase reduces to less than 2%, while bainitic ferrite increases from 15.5 to 32.6%.

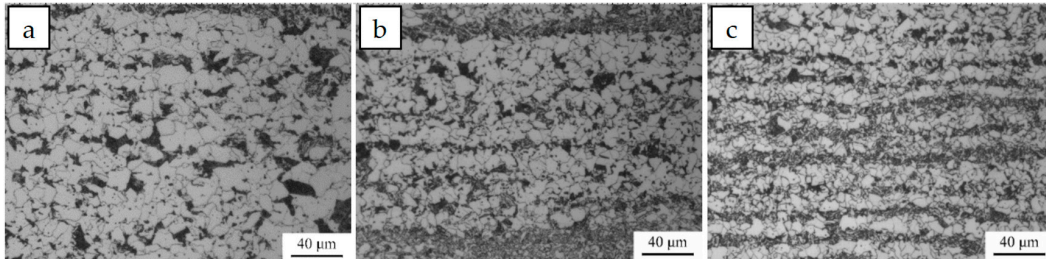


Figure 2. Morphology of normalized steel samples: (a) 36N; (b) 103N; (c) 165N.

Figure 3a shows the TEM images of samples with different N contents. The pearlite in the 36N sample exhibits a distinct lamellar structure (Figure 3a). However, in the 103N sample, the pearlite degenerates, and a striped feature of bainite appears (Figure 3b). The black component in the 165N sample is bainite instead of pearlite (Figure 3c). As the N content increases, pearlite gradually degenerates and eventually transforms into bainitic ferrite.

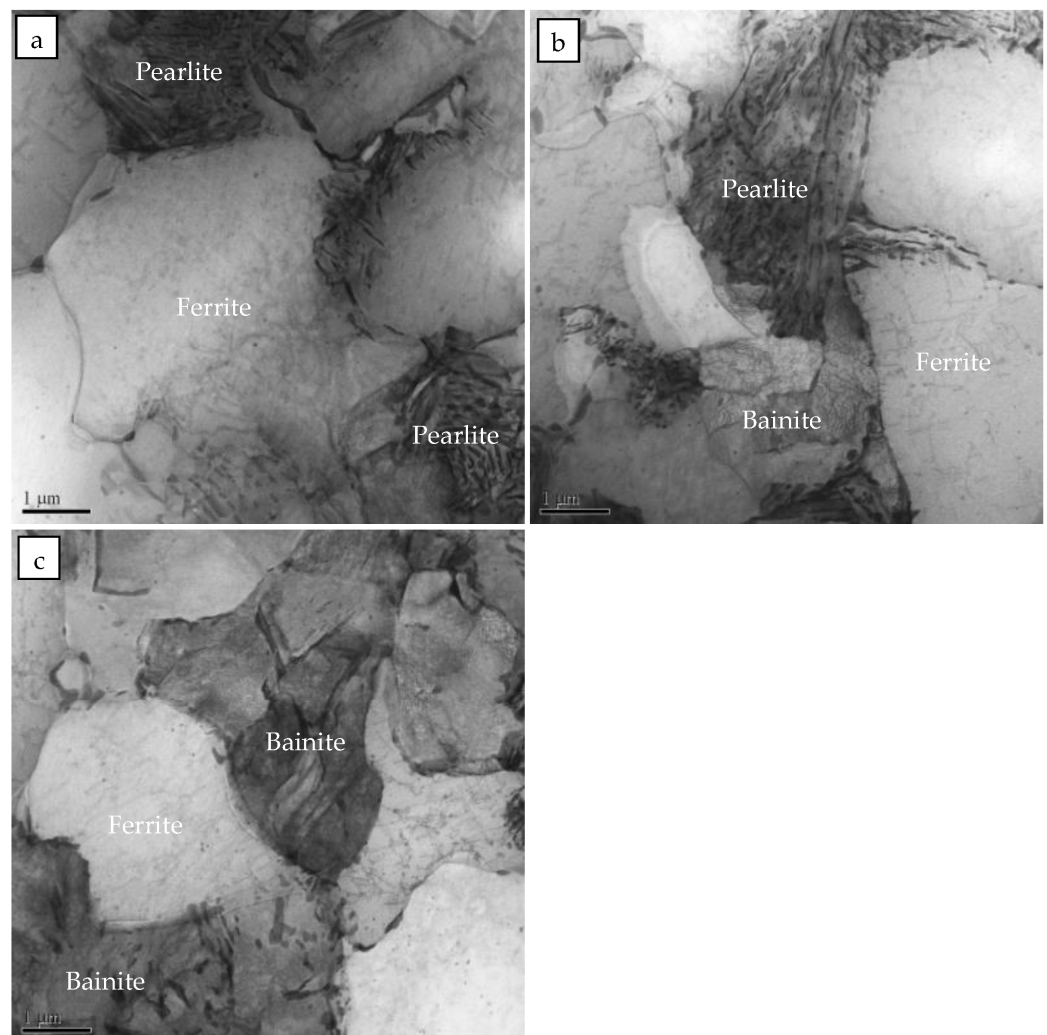


Figure 3. TEM of normalized steel samples with different N contents: (a) 36N; (b) 103N; (c) 165N.

Several studies have shown that the effective grain size defined at 15° is an effective measure for controlling crack propagation. Figure 4 shows inverse pole maps of steel samples with different N contents. The black line in the maps represents the high-angle boundary with a misorientation tolerance angle of $\geq 15^\circ$. The change in the effective grain size defined at 15° with N content is shown in Figure 5a. As indicated, the 165N sample possesses the finest effective grain size. When the N content increases from 36 ppm to 165 ppm, the average grain size of ferrite defined by the 15° angle decreases from $12.3 \mu\text{m}$ to $6.7 \mu\text{m}$. Figure 5b shows the proportion of grain boundaries defined at different misorientation angles for samples with different N contents. With the increase in N content, the proportion of high-angle boundaries increases, while the proportion of small-angle boundaries decreases. The areal density of high-angle boundaries increases from $0.13/\mu\text{m}$ to $0.49/\mu\text{m}$. All the above changes can be attributed to the refinement of the ferrite microstructure.

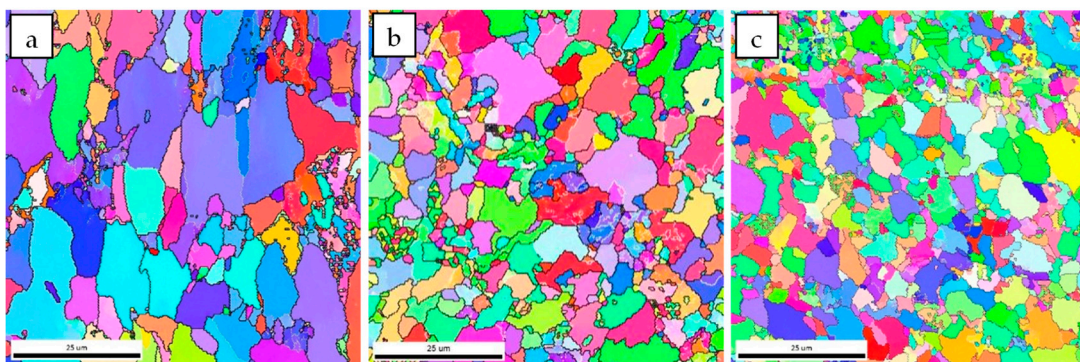


Figure 4. Inverse pole figures of different N content samples normalized at 900°C : (a) 36N; (b) 103N; (c) 165N.

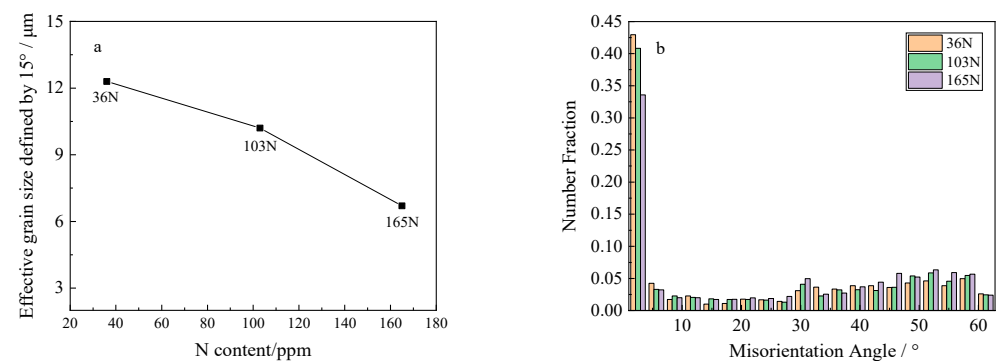


Figure 5. (a) Effect of N content on effective grain size defined as 15° ; (b) distribution of microstructure boundary misorientation in the normalized 36N, 103N, and 165N steel samples.

3.2. Effect of N Content on the Mechanical Properties of Steel Samples

The results of the tensile test and impact test are summarized in Table 2. The strengths of the three experimental steels with varying N content meet the technical requirements of P460NL1. However, the impact toughness is poor at lower N content and does not meet the technical specifications of P460NL1. The impact energy of 36N, 103N, and 165N samples is 34 J, 48 J, and 88 J, respectively. With the increase in N content, the impact toughness of the steel samples significantly improves. Therefore, this study does not focus on the tensile properties but instead concentrates on the effect of N content on the impact toughness of the experimental steels.

Figure 6 shows the fracture morphology characteristics of impacted samples. Figure 6a–c depicts the impact fracture overviews of 36N, 103N, and 165N samples, respectively. The area of the fiber zones in impact samples with different N contents was measured via Image-pro

plus 6.0 software. The results showed that the fracture fiber rates for the 36N, 103N, and 165N samples were 7%, 15%, and 26%, respectively. Higher N content gradually enhances the fracture fiber rate of impacted samples. Figure 6d depict the morphology of the fracture fiber zone, while Figure 6g depicts the propagation zone for sample 36N. The fiber zone of the impact fracture in the 36N sample consists of fine and shallow dimples, while the propagation zone is mainly composed of the larger and flat cleavage planes. Figure 6e show the morphology of the fracture fiber zone for sample 103N, while Figure 6h shows its propagation zone. The fiber zone of the impact fracture of the 103N sample exhibits fine and shallow dimples, while the propagation zone consists of smaller and uneven cleavage planes compared to the 36N sample. Finally, Figure 6f display the morphology of the fracture fiber zone, while Figure 6i displays the propagation zone for sample 165N. The fiber zone of the impact fracture in the 165N sample exhibits fine and deep dimples, and the propagation zone contains smaller cleavage planes. In contrast to the 36N and 103N samples, the cleavage plane of the 165N sample has a greater surface roughness, and a few tearing edges can be observed in the dimples between some of the cleavage planes. These results indicate that the enhanced N content in V micro-alloyed steel transforms the fracture behavior from brittle fracture to mixed fracture.

Table 2. Summary of the mechanical properties of steel with different N contents.

Steel	Impact Energy/J			Average Value/J	Yield Stress/MPa	Tensile Strength/MPa	Tensile Elongation
36N	31	36	35	34	479	636	28.5
103N	45	49	50	48	495	653	26.3
165N	83	89	92	88	513	670	21.7

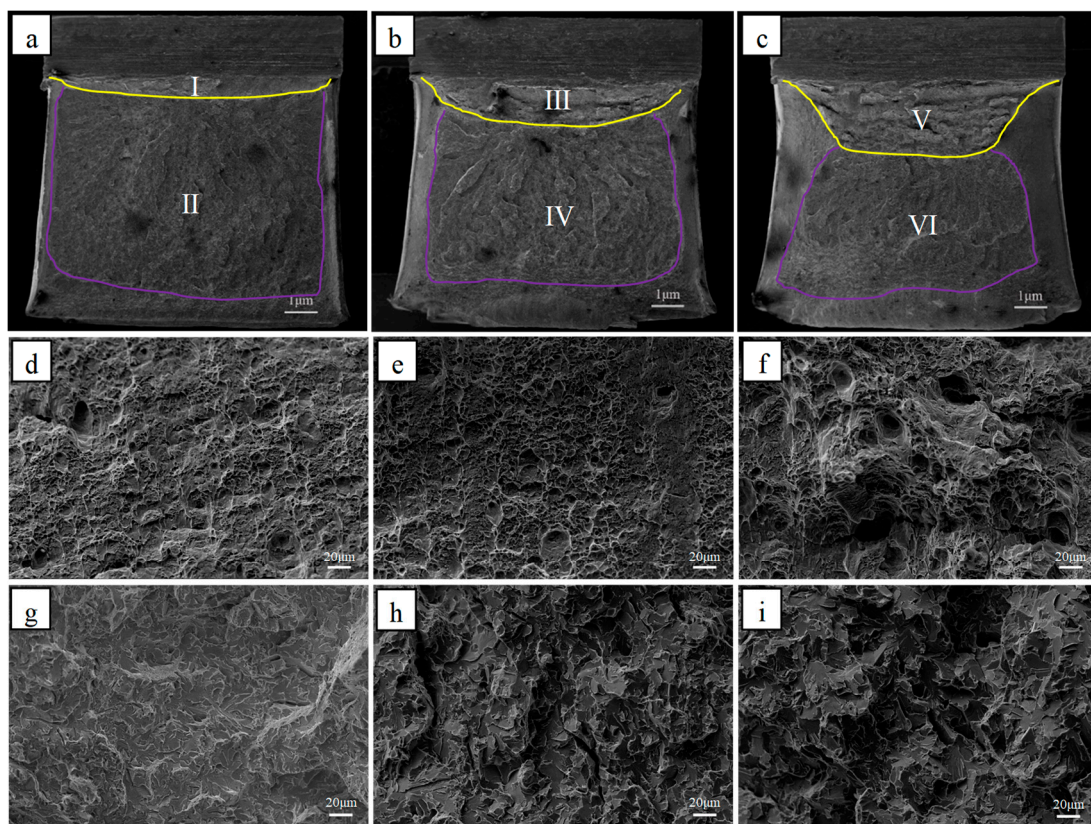


Figure 6. Impact fracture morphology of 36N (a), 103N (b), and 165N (c) at $-40\text{ }^{\circ}\text{C}$. Characterization (d/g, e/h, and f/i) of the position marked as I/II in 36N (a), as III/IV in 103N (b), and as V/VI in 165N (c), respectively.

4. Discussion

4.1. Analysis of the Microstructures of Steel Samples

As in previous studies, the grain size of normalized steel is associated with the prior austenite grain size. By refining the prior austenite grain size, the microstructure of normalized steel is significantly refined. During the transition from austenite to ferrite, V (C,N) particles with a size of $\sim 0.2 \mu\text{m}$ in V-Ti micro-alloyed steel can act as ferrite nucleation sites, which promotes ferrite nucleation [20,21]. N doping influences the components and contents of V (C,N) precipitated particles in V micro-alloyed steel [22]. Hou Hong et al. [14] studied the effect of N content on the microstructure and impact toughness of normalized steel, but they did not characterize the relationship between precipitates and microstructure. To explore the effect of N content on the microstructures of vanadium micro-alloyed P460NL1 steel sheets, a normalizing treatment process was simulated using the Gleeble 3800 thermal simulator. Water quenching was carried out during the air-cooling process to observe the evolution of steel's microstructure. Additionally, SEM equipped with EDS was employed to study the role of precipitated particles in phase transitions.

Figure 7 shows the microstructure morphology in the 36N and 165N samples when water-quenched at 880°C . As shown in Figure 7a, the microstructure is lath bainite, which means that the austenite remains unchanged in the 36N when the sample is cooled from 900°C to 880°C . The austenite transforms into lath bainite during quenching, retaining most of the primitive austenite grain boundaries. When the 165N sample is cooled from 900°C to 880°C , the phase transition from austenite to ferrite preferentially occurs at the prior austenite boundary (Figure 7b). Consequently, the prior austenite grain size can be inferred from the context of ferrite. As shown in Figure 7, the area surrounded by the yellow line indicates a prior austenite grain. The prior austenite grain size of the 165N sample is about half that of the 36N sample. With the increase in N content in the steel samples from 36 ppm to 165 ppm, a significant refinement occurs in the prior austenite grains.

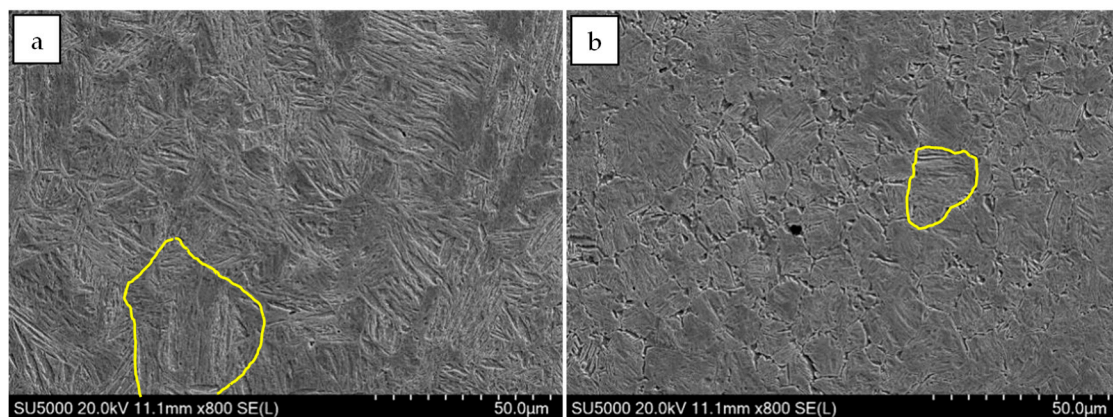


Figure 7. SEM images of (a) 36N and (b) 165N samples water-quenched at 880°C .

Figure 8b depicts a high-magnification image of the red square area shown in Figure 8a. In Figure 8b, it can be observed that ferrite forms on the V (C,N) particles near the prior austenite boundary, creating fine boundary ferrite. The size of the V (C,N) particles that promote ferrite nucleation at the prior austenite boundary in the 165N sample is about 70 nm , indicating that the V (C,N) particles are not completely dissolved during normalizing [22]. During the cooling process, the undissolved V (C,N) particles at the boundary provide a favorable site for ferrite nucleation, thereby enhancing ferrite nucleation.

Figure 9 shows TEM images of the 165N sample after incubation at 900°C for 30 min. Figure 9b shows an enlarged view of the prior austenite boundary (as shown in the red box in Figure 9a). Spectrum1 and Spectrum2 are the energy spectra of particles 1 and 2 marked by red arrows in Figure 9b, respectively. According to energy spectrum results, fine V (C,N) precipitated particles are observed on the prior austenite boundary. During

normalizing at 900 °C, undissolved V (C,N) precipitated particles can effectively pin the primitive austenite boundary and inhibit the growth of prior austenite grains.

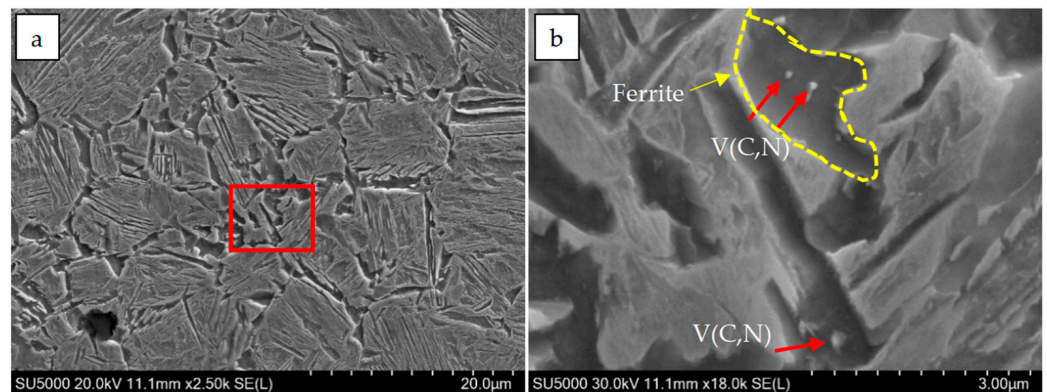


Figure 8. Nucleation of ferrite at the prior austenite boundary in the 165N sample: (a) overview of the matrix microstructure; (b) enlarged view of the red box zone.

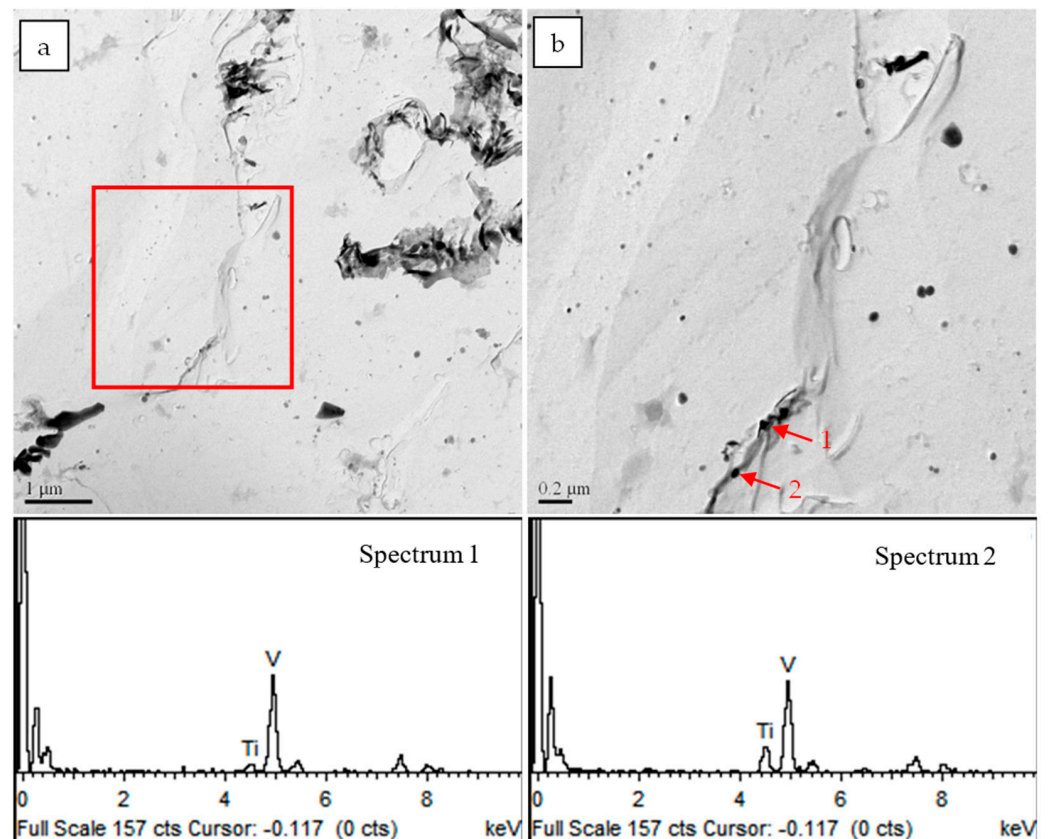


Figure 9. TEM micrographs showing precipitates (indicated by arrows) along grain boundaries in carbon extraction replicas of the 165 N sample at a quenching temperature of 900 °C (a). Enlarged view of the red box zone (b).

Figure 10 shows the precipitated particles in the 36N and 165N experimental steels. Figure 10a,b show that there are many fine V (C,N) particles in the rolled-state steels. After holding at 900 °C for 30 min, most of the fine V (C,N) particles in the 36N sample dissolved, while a significant number of fine V (C,N) particles still existed in the 165N sample. The dissolved V (C,N) reprecipitated during the cooling process of normalization in the 36N specimen, resulting in the reappearance of fine V (C,N), as shown in Figure 10e. The size of the precipitated particles in Figure 10f is larger than that in Figure 10d. This is due to

the V (C,N) particles preferentially precipitating and attaching to the undissolved particles during the cooling process.

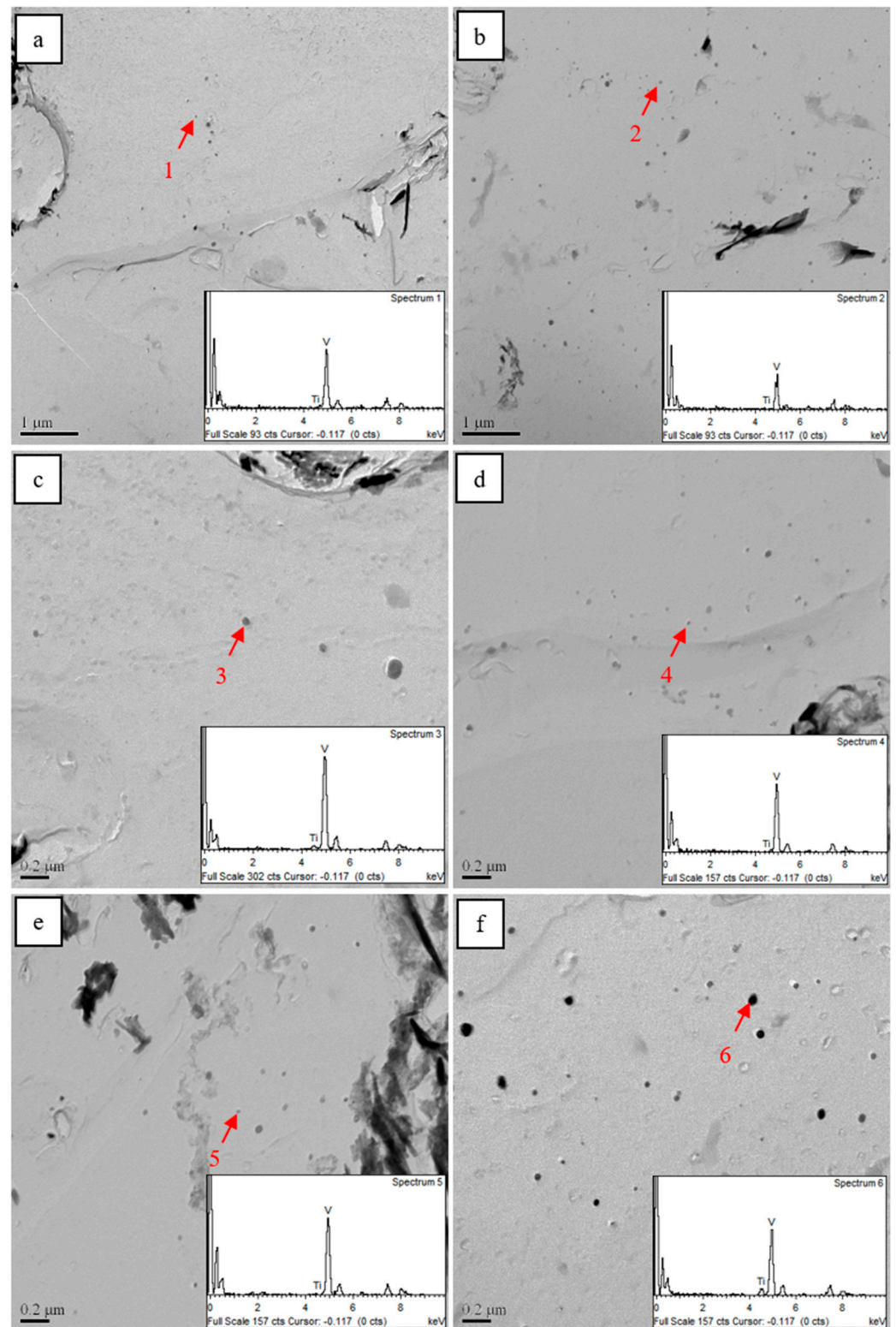


Figure 10. Observation of precipitated particles in the 36N and 165N samples: (a,c,e) 36N sample and (b,d,f) 165N sample; (a,b) rolled state; (c,d) water-quenched at 900 °C; and (e,f) normalized.

According to the thermodynamic calculations (Figure 11), an increase in N content from 36 ppm to 165 ppm raises the dissolution–precipitation temperature of V (C,N),

i.e., from 1053 °C to 1135 °C. Additionally, the volume fraction of V (C,N) particles in steel samples increases from 5.3×10^{-4} to 11.4×10^{-4} at 900 °C. Between 900 °C and 910 °C, the volume fraction of precipitated particles in the 165N sample is about twice that of the precipitated particles in the 36 N sample. Furthermore, the addition of N changes the specific gravity of C and N atoms in V (C,N) precipitated particles, making V (C,N) particles more stable and less likely to dissolve [22]. As shown in Figure 11b, the percentage of N in V (C,N) precipitated particles in the 165N sample is higher than that in V (C,N) precipitated particles in the 36N sample. The higher the N content in V (C,N) particles, the higher the thermal stability of the particles. Thus, the particles in the 165N samples are less likely to dissolve during normalizing. This observation is consistent with the trend observed in TEM characterization (Figure 10).

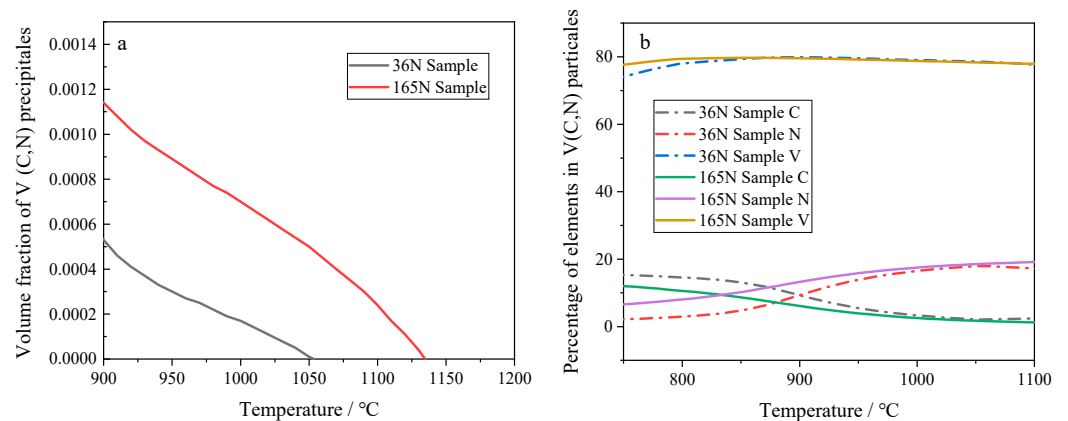


Figure 11. Volume fractions of precipitates (a) and precipitated particle composition in the 36N and 165N samples (b).

Figure 12 shows SEM images of 165N normalized samples. As observed, the precipitated particles in the 165N normalized samples are located near the center of the ferrite interior, and their size is noticeably larger than that of the samples water-quenched at 900 °C, implying that the precipitated particles grew during cooling. They form 0.2 μm V (C,N) particles, which exhibit a strong ability to promote the nucleation of ferrite and provide more favorable positions for ferrite nucleation during the cooling process [23]. This refinement enhances the microstructure of vanadium micro-alloyed P460NL1 steel.

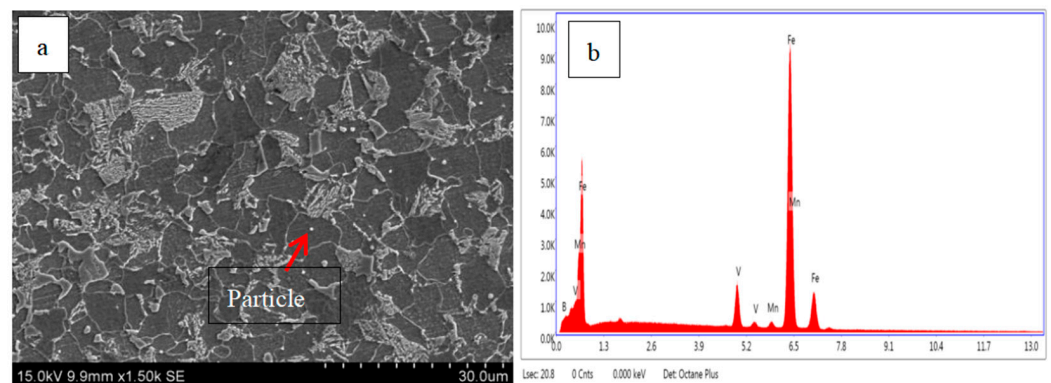


Figure 12. SEM images of a 165N normalized sample (a) and the energy spectrum of precipitated particle (b).

With the increase in N content, both the number of precipitated particles that can pin the original austenite grain boundaries during the normalizing process and the number of precipitated particles that can provide nucleation sites for the ferrite transformation in the cooling process have increased. Therefore, as the N content increases, the microstructure of the test steel undergoes refinement.

4.2. Impact Toughness of Steel Samples

As N doping increases from 36 ppm to 165 ppm, the impact energy of normalized vanadium micro-alloyed P460NL1 steel increases from 34 to 88 J. The failure mode changes from brittle failure to mixed failure. According to fracture mechanics, impact energy can be categorized into crack initiation energy and crack propagation energy. Thus, the effect of N on the impact performance of normalized V micro-alloyed P460NL1 steel is investigated from the perspective of crack initiation and propagation.

Numerous studies have shown that impact toughness is related to the second phase (martensite/austenite elements and pearlite), grain size, and microstructure composition [24–26]. The difference in thermal expansion coefficients between pearlite and ferrite results in varying degrees of shrinkage of these two components during the cooling process, leading to a certain degree of strain within or around the pearlite. The strain causes localized stress concentrations in or around the pearlite microstructure. The kernel average misorientation plot can be used to evaluate the magnitude of the strain. The band contrast map and the kernel average misorientation plot of the 36N and 165N samples are shown in Figure 13.

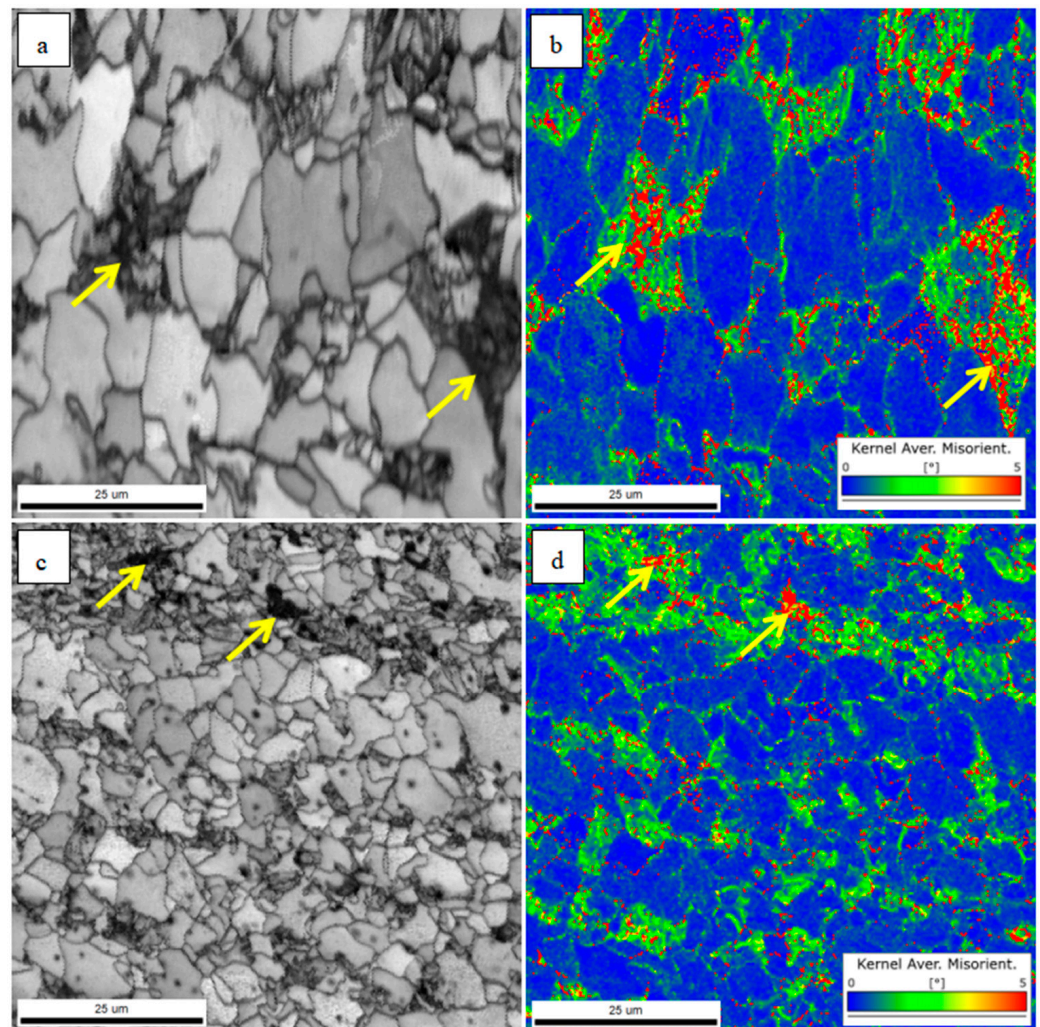


Figure 13. Band contrast map and kernel average misorientation map of the 36N sample (a,b) and 165N sample (c,d).

In both the 36N and 165N samples, strain occurs within the pearlite microstructure or at the pearlite–ferrite matrix interface (indicated by the yellow arrow in Figure 13). This strain increases with the growing size of pearlite. As the N content in V micro-alloyed steel

P460NL1 increases from 36 to 165 ppm, the number of pearlite components and the size of pearlite components decrease (Figure 2). Consequently, the 165N normalized samples exhibit minimal strain near pearlite.

The crack initiation and crack propagation of the 36N and 165N samples are shown in Figure 14a,c, where cracks develop near pearlite due to the presence of stress inside or around the pearlite structure. Under the action of an impact load, the uncoordinated deformation of pearlite and the surrounding matrix microstructure further aggravate the stress concentration inside or around the pearlite structure [25,27]. According to fracture theory, crack initiation occurs when the local stress concentration exceeds the critical stress. Previous studies have demonstrated that high critical stress is required for crack initiation when the hard-phase component reduces in size [28]. As the pearlite microstructure in the 165N sample is both smaller and less abundant, the micro-crack initiation of the 165N sample consumes more energy than that of the 36N sample.

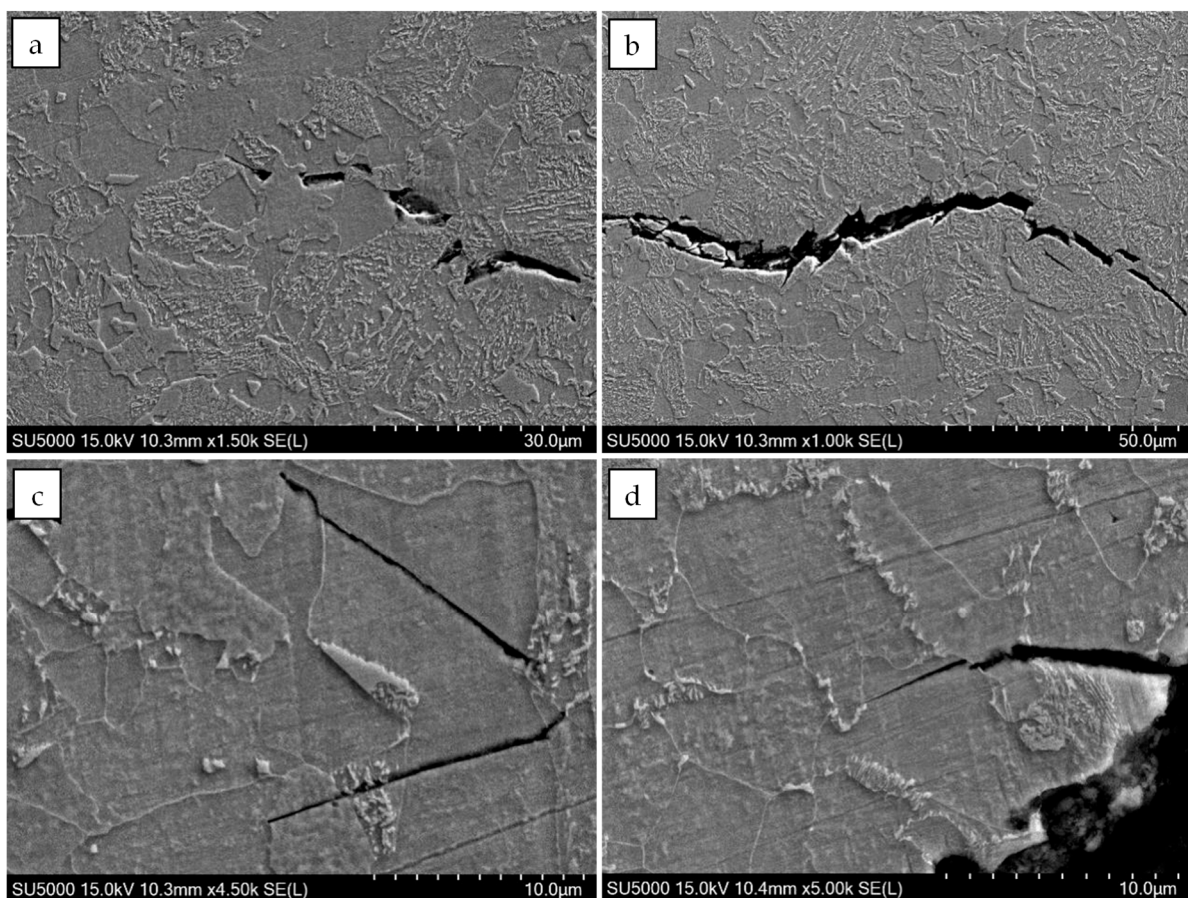


Figure 14. SEM observation of crack initiation and crack propagation in 36N (a,b) and 165N (c,d) samples.

The spatial distribution of microstructure and high-angle boundaries greatly influences crack propagation [16,29,30]. Figure 14b,d show the crack propagation paths of the 36N and 165N samples, respectively. The high content of pearlite microstructure and the limited inhibitory effect of pearlite on crack propagation led to the formation of coarse and long cracks in the 36N sample (Figure 13b). In contrast, the crack length in the 165N sample is shorter. The 165N sample contains less pearlite content, i.e., it mainly consists of fine ferrite. The ferrite possesses strong deformation ability due to its soft nature and low yield strength. The cracks consume more energy when passing through the ferrite, causing the cracks to suddenly become narrower (Figure 14d).

Figure 15 shows the EBSD patterns of the secondary cracks in the 165N sample. In the figure, the red line represents the high-angle boundary (HAGB) defined at 15° . The cracks pass through the interior of the grains without deflection, indicating that crack propagation inside the grains experiences negligible resistance. However, when the cracks encounter HAGBs, the crack propagation direction changes, which is eventually captured at HAGBs. In summary, HAGBs ($\theta > 15^\circ$) can be an effective obstacle for crack propagation. In the 165N sample, ferrite grains are fine, and HAGB spacing is short. As a result, the cracks are deflected multiple times during crack propagation, as shown in Figure 15.

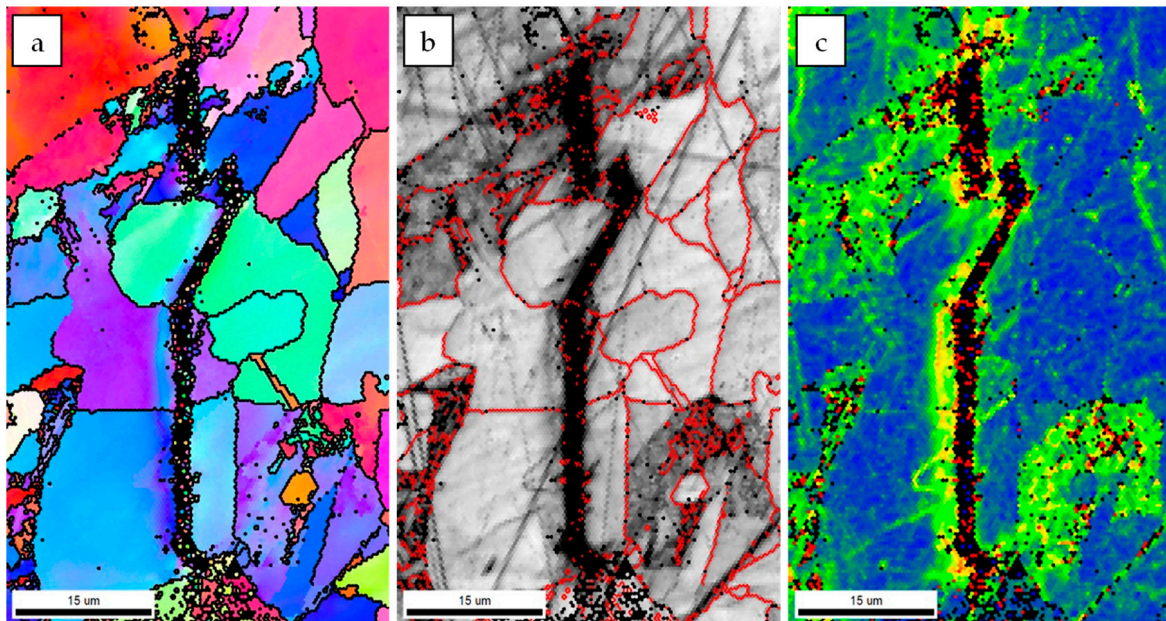


Figure 15. Inverse pole figures (a), band contrast map (b), and kernel average misorientation map (c) of cleavage crack propagation paths in the 165N sample.

The high deformability of ferrite absorbs crack propagation energy and converts it into internal strain, thereby hindering crack propagation (Figure 15c). As the doping of N increases from 36 ppm to 165 ppm, the pearlite microstructure in V micro-alloyed P460NL1 steel decreases. As the effective grain size of ferrite refines, the number of high-angle boundaries increases significantly, resulting in enhanced propagation resistance and the consumption of more energy during the crack propagation process. This improves the impact toughness of vanadium micro-alloyed P460NL1 steel.

The doping of N in vanadium micro-alloyed P460NL1 steel reduces the pearlite microstructure, resulting in a more dispersed and finer size of pearlite. Higher N doping promotes the precipitation of V in the steel, forming more V (C,N) particles. The undissolved V (C,N) particles in the normalizing process pin the prior austenite grains, which inhibits their growth. During air cooling, V (C,N) particles provide nucleation sites for ferrite, which stimulate ferrite nucleation and refine the microstructure. This significantly improves the impact toughness of V micro-alloyed P460NL1 steel.

5. Conclusions

- (1) Doping of N in vanadium micro-alloyed P460NL1 steel can transform coarse ferrite and pearlite blocks into fine ferrite and bainitic ferrite blocks.
- (2) High N doping (165ppm) promoted the precipitation of V (C,N) particles in V micro-alloyed P460NL1 steel, leading to the formation of more fine V (C,N) particles and improving the stability of V (C,N) particles. The fine and stable V (C,N) particles in the normalizing process can effectively pin the prior austenite boundary and refine the prior austenite grains. During cooling, V (C,N) particles induced ferrite nucleation, resulting in fine ferrite.

- (3) As the N content increased from 36 ppm to 165 ppm in vanadium micro-alloyed P460NL1 steel, the impact toughness of the steel significantly increased from 34 J to 88 J, and the failure pattern changed from brittle failure to mixed failure.

Author Contributions: Investigation, Q.W. (Qiuming Wang); Data curation, H.F.; Writing—original draft, X.L.; Writing—review & editing, Q.W. (Qingfeng Wang). All authors have read and agreed to the published version of the manuscript.

Funding: This work was supported by the National Natural Science Foundation of China (52127808) and the Innovation Ability Promotion Program of Hebei (22567609H).

Data Availability Statement: Data is contained within the article. The data presented in this study are available in [Effect of N Content on Microstructure and Impact Properties of Normalized Vanadium Micro-Alloyed P460NL1 Steel].

Conflicts of Interest: Author Xinliang Li was employed by the company Nanjing Iron & Steel Co., Ltd. The remaining authors declare that the research was conducted in the absence of any commercial or financial relationships that could be construed as a potential conflict of interest.

References

1. Ouchi, C. Advances in Physical Metallurgy and Processing of Steels. Development of Steel Plates by Intensive Use of TMCP and Direct Quenching Processes. *ISIJ Int.* **2001**, *41*, 542–553. [[CrossRef](#)]
2. Moss, D.R.; Basic, M.M. *Pressure Vessel Design Manual*; Elsevier: Amsterdam, The Netherlands, 1987.
3. Tong, M.W.; Yuan, Z.X.; Zhang, K.G. Influence of Vanadium on Microstructures and Mechanical Properties of High Strength Normalized Steel. *Adv. Mater. Res.* **2012**, *535*, 628–632. [[CrossRef](#)]
4. Pan, T.; Chai, X.; Wang, J.; Su, H.; Yang, C. Precipitation Behavior of V-N Microalloyed Steels during Normalizing. *J. Iron Steel Res. Int.* **2015**, *22*, 1037–1042. [[CrossRef](#)]
5. Pindor, L.; Matějka, V.; Kozelsky, P.; Michalek, K.; Gigacher, G. Investigation into Secondary Phases in Steels Microalloyed with Vanadium and Nitrogen. *Ironmak. Steelmak.* **2013**, *35*, 124–128. [[CrossRef](#)]
6. Medina, S.F.; Gómez, M.; Rancel, L. Grain Refinement by Intragranular Nucleation of Ferrite in a High Nitrogen Content Vanadium Microalloyed Steel. *Scr. Mater.* **2008**, *58*, 1110–1113. [[CrossRef](#)]
7. Zhang, Z.H.; Liu, Y.; Zhou, Y.N.; Dong, X.M.; Zhang, C.X.; Cao, G.H.; Schneider, R.; Gerthsen, D. Effect of Precipitation of (Ti,V)N and V(C,N) Secondary Phases on Mechanical Properties of V and N Microalloyed 1Cr Steels. *Mater. Sci. Eng. A* **2018**, *738*, 203–212. [[CrossRef](#)]
8. Xie, Z.; Hui, W.; Bai, S.; Zhang, Y.; Zhao, X.; Li, B. Effects of Annealing Temperature and V Addition on Microstructure and Mechanical Properties of Fe-Mn-Al-C Austenitic Low-Density Steel. *Mater. Today Commun.* **2023**, *35*, 106328. [[CrossRef](#)]
9. Zhao, X.; Zhao, K.; Liu, C.; Yang, Z.; Zhang, F. Effect of Ausforming on the Bainitic Transformation and Microstructure in Medium Carbon V-N Micro-Alloyed Steel. *J. Mater. Res. Technol.* **2023**, *23*, 637–647. [[CrossRef](#)]
10. Li, L.; Song, B.; Cui, X.; Liu, Z.; Wang, L.; Cheng, W. Effects of Finish Rolling Deformation on Hydrogen-Induced Cracking and Hydrogen-Induced Ductility Loss of High-Vanadium TMCP X80 Pipeline Steel—ScienceDirect. *Int. J. Hydrogen Energy* **2020**, *45*, 30828–30844. [[CrossRef](#)]
11. Liang, X.; Shen, J.; Jiao, S.; Wang, C. Precipitation Behavior of Vanadium in a High Nitrogen and Vanadium Bearing Steel Treated with TMCP. In *Materials Science & Technology Conference and Exhibition: Product Manufacturing*; John Wiley & Sons: Hoboken, NJ, USA, 2006.
12. Xia, Z.X.; Zhang, C.; Yang, Z.G. Control of Precipitation Behavior in Reduced Activation Steels by Intermediate Heat Treatment. *Mater. Sci. Eng. A* **2011**, *528*, 6764–6768. [[CrossRef](#)]
13. Tao, P.; Zhang, C.; Yang, Z.G.; Hiroyuki, T. Evolution and Coarsening of Carbides in 2. 25Cr1Mo Steel Weld Metal During High Temperature Tempering. *J. Iron Steel Res. Int.* **2010**, *17*, 74–78. [[CrossRef](#)]
14. Hong, H.; Chunming, L.; Hanqian, Z. Effect of N Content on Microstructure and Properties of Normalized Steel for Mobile Containers. *J. Chin. Core J. Criterion PKU Press. Vessel.* **2019**, *36*, 1–7.
15. Medina, S.F.; Rancel, L.; Gómez, M.; Ishak, R.; De Sanctis, M. Intragranular Nucleation of Ferrite on Precipitates and Grain Refinement in a Hot Deformed V-Microalloyed Steel. *ISIJ Int.* **2008**, *48*, 1603–1608. [[CrossRef](#)]
16. Fan, H.; Shi, G.; Peng, T.; Wang, Q.; Wang, L.; Wang, Q.; Zhang, F. N-Induced Microstructure Refinement and Toughness Improvement in the Coarse Grain Heat-Affected Zone of a Low Carbon Mo-V-Ti-B Steel Subjected to a High Heat Input Welding Thermal Cycle. *Mater. Sci. Eng. A* **2021**, *824*, 141799. [[CrossRef](#)]
17. Garcia-Mateo, C.; Capdevila, C.; Caballero, F.G.; Andres, C.G.D. Influence of V Precipitates on Acicular Ferrite Transformation Part 1: The Role of Nitrogen. *ISIJ Int.* **2008**, *48*, 1270–1275. [[CrossRef](#)]
18. Sun, L.; Zhang, S.; Song, R.; Ren, S.; Zhang, Y.; Sun, X.; Dai, G.; Hao, Y.; Huo, W.; Zhao, S.; et al. Effect of V, Nb, and Ti Microalloying on Low-Temperature Impact Fracture Behavior of Non-Quenched and Tempered Forged Steel. *Mater. Sci. Eng. A* **2023**, *879*, 145299. [[CrossRef](#)]

19. Pickering, F. *High-Strength, Low Alloy Steels—A Decade of Progress*; Union Carbide Corp: New York, NY, USA, 1975.
20. Ricks, R.A.; Howell, P.R.; Barritte, G.S. The Nature of Acicular Ferrite in HSLA Steel Weld Metals. *J. Mater. Sci.* **1982**, *17*, 732–740. [[CrossRef](#)]
21. Hu, J.; Du, L.X.; Wang, J.J.; Gao, C.R. Effect of Welding Heat Input on Microstructures and Toughness in Simulated CGHAZ of V–N High Strength Steel. *Mater. Sci. Eng. A* **2013**, *577*, 161–168. [[CrossRef](#)]
22. Fang, F.; Qi-Long, Y.; Cai-Fu, Y.; Hang, S.U. Microstructure and Precipitation Behavior in Heat Affected Zone of Nitrogen-Enhanced Microalloyed Steel Containing V and Ti. *J. Iron Steel Res. Int.* **2007**, *14*, 249–253. [[CrossRef](#)]
23. Hu, J.; Du, L.X.; Wang, J.J. Effect of V on Intragranular Ferrite Nucleation of High Ti Bearing Steel. *Scr. Mater.* **2013**, *68*, 953–956. [[CrossRef](#)]
24. Contribution of Grain Size to Resistance against Cleavage Crack Propagation in Ferritic Steel—ScienceDirect. Available online: <https://www.sciencedirect.com/science/article/abs/pii/S1359645419304112?via%3Dihub> (accessed on 21 June 2019).
25. Mohseni, P.; Solberg, J.K.; Karlsen, M.; Akselsen, O.M.; Østby, E. Investigation of Mechanism of Cleavage Fracture Initiation in Intercritically Coarse Grained Heat Affected Zone of HSLA Steel. *Mater. Sci. Technol.* **2012**, *28*, 1261–1268. [[CrossRef](#)]
26. Han, J.; Da Silva, A.K.; Ponge, D.; Raabe, D.; Lee, S.M.; Lee, Y.K.; Lee, S.I.; Hwang, B. The Effects of Prior Austenite Grain Boundaries and Microstructural Morphology on the Impact Toughness of Intercritically Annealed Medium Mn Steel. *Acta Mater.* **2017**, *122*, 199–206. [[CrossRef](#)]
27. Zhang, S.; Romo, S.; Giorjao, R.A.; Leao, P.B.P.; Ramirez, A.J. EBSD Analysis of Strain Distribution and Evolution in Ferritic-Pearlitic Steel under Cyclic Deformation at Intermediate Temperature. *Mater. Charact.* **2022**, *193*, 112293. [[CrossRef](#)]
28. Shi, G.; Luo, B.; Zhang, S.; Wang, Q.; Zhao, H. Microstructural Evolution and Mechanical Properties of a Low-Carbon V-N-Ti Steel Processed with Varied Isothermal Temperatures. *Mater. Sci. Eng. A* **2021**, *801*, 140396. [[CrossRef](#)]
29. Rodriguez-Ibabe, J.M. The Role of Microstructure in Toughness Behaviour of Microalloyed Steels. In *Materials Science Forum*; Trans Tech Publications Ltd.: Bäch, Switzerland, 1998; Volume 284, pp. 51–62. [[CrossRef](#)]
30. Wang, K.; Hu, F.; Zhou, S.; Zhou, W.; Hu, C.; Yershov, S.; Wu, K. Microstructural Evolution and Ultra-High Impact Toughness of Austempered Lamellar Bainitic Steel Far below Ms Temperature. *J. Mater. Res. Technol.* **2023**, *24*, 5449–5462. [[CrossRef](#)]

Disclaimer/Publisher’s Note: The statements, opinions and data contained in all publications are solely those of the individual author(s) and contributor(s) and not of MDPI and/or the editor(s). MDPI and/or the editor(s) disclaim responsibility for any injury to people or property resulting from any ideas, methods, instructions or products referred to in the content.